Journal of Integrative Agriculture 2021, 20(12): 3240–3255

Available online at www.sciencedirect.com

ScienceDirect

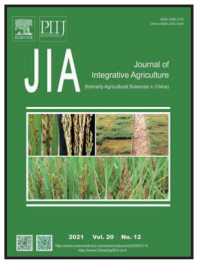

RESEARCH ARTICLE

Functional identification of C-type lectin in the diamondback moth, *Plutella xylostella* (L.) innate immunity

LI Jin-yang[1, 2, 3], LIN Jun-han[1, 2, 3, 4], G. Mandela FERNÁNDEZ-GRANDON[5], ZHANG Jia-yu[1, 2, 3], YOU Min-sheng[1, 2, 3], XIA Xiao-feng[1, 2, 3]

[1] *State Key Laboratory of Ecological Pest Control for Fujian and Taiwan Crops, Institute of Applied Ecology, Fujian Agriculture and Forestry University, Fuzhou 350002, P.R.China*

[2] *Joint International Research Laboratory of Ecological Pest Control, Ministry of Education, Fuzhou 350002, P.R.China*

[3] *Key Laboratory of Integrated Pest Management for Fujian-Taiwan Crops, Ministry of Agriculture and Rural Affairs, Fuzhou 350002, P.R.China*

[4] *Fujian Vocational College of Bioengineering, Fuzhou 350002, P.R.China*

[5] *Natural Resources Institute, University of Greenwich, Kent ME4 4TB, UK*

Abstract

C-type lectins (CTLs) are a superfamily of Ca^{2+}-dependent carbohydrate-recognition proteins, and an important pattern recognition receptor (PRR) in insect innate immunity which can mediate humoral and cellular immunity in insects. In this study, we report a novel dual carbohydrate-recognition domain (CRD) CTL from *Plutella xylostella* which we designate PxIML. PxIML is a protein with a 969 bp open reading frame (ORF) encoding 322 amino acids, containing a signal peptide and a dual-CRD with EPN (Glu_{124}-Pro_{125}-Asn_{126}) and QPD (Gln_{274}-Pro_{275}-Asp_{276}) motifs. The expression of *PxIML* mRNA in the fat body was significantly higher than in hemocytes and midgut. The relative expression levels of *PxIML* in the whole insect and the fat body were significantly inhibited after infection with *Bacillus thuringiensis* 8010 (Bt8010) at 18 h, while they were significantly upregulated after infection with *Serratia marcescens* IAE6 or *Pichia pastoris*. The recombinant PxIML (rPxIML) protein could bind to the tested pathogen-associated molecular patterns (PAMPs), and the bacteria of *Enterobacter* sp. IAE5, *S. marcescens* IAE6, *Staphylococcus aureus*, *Escherichia coli* BL21, and Bt8010 in a Ca^{2+}-dependent manner, however, it showed limited binding to the fungus, *P. pastoris*. The rPxIML exhibited strong activity in the presence of Ca^{2+} to agglutinate Bt8010, *Enterobacter* sp. IAE5 and *S. aureus*, but it only weakly agglutinated with *E. coli* BL21, and could not agglutinate with *S. marcescens* IAE6 or *P. pastoris*. Furthermore, the rPxIML could bind to hemocytes, promote the adsorption of hemocytes to beads, and enhance the phenoloxidase (PO) activity and melanization of *P. xylostella*. Our results suggest that PxIML plays an important role in pathogen recognition

Received 22 September, 2020 Accepted 20 February, 2021
LI Jin-yang, E-mail: 15298075245@163.com; Correspondence YOU Min-sheng, E-mail: msyou@fafu.edu.cn; XIA Xiao-feng, Tel: +86-591-83856841, E-mail: xiaofengxia@fafu.edu.cn

doi: 10.1016/S2095-3119(21)63650-X

and in mediating subsequent humoral and cellular immunity of *P. xylostella*.

Keywords: diamondback moth, humoral and cellular immunity, C-type lectin, pattern recognition receptors, carbohydrate-recognition domain

1. Introduction

The success of insects in adapting to various ecological environments is partly due to their ability to resist pathogens and parasites (Lowenberger *et al.* 1999). Insects lack an acquired immune system mediated by lymphocytes, but have a well-developed innate immune system to defend against pathogens (Lavine and Strand 2002). The innate immune response is initiated by the recognition of molecules on the surface of pathogens, which are called pathogen-associated molecular patterns (PAMPs) (Huang *et al.* 2015). PAMPs are conserved molecules on the surface of pathogens, mainly composed of the cell wall components of fungi and bacteria, including peptidoglycan (PGN), lipopolysaccharide (LPS), flagellin, β-1,3-glucan, mannose (Man), lipopeptides and lipoteichoic acid (LTA), and other similar associated components (Zheng and Xia 2012). The pattern recognition receptor (PRR) is a kind of protein encoded by the germline, which can bind to PAMPs and induce various downstream immune reactions (Sullivan and Belloir 2014; Zhang *et al.* 2015). At present, many types of PRRs have been found in insects, including peptidoglycan recognition protein (PGRP), β-1,3-glucan recognition proteins (βGRP), Gram-negative bacteria binding protein (GNBP), scavenger receptor (SCR), hemolin (HEM), apolipophorin (apoLp), thioester-containing protein (TEP), C-type lectin (CTL), Toll, integrins and Down syndrome cell adhesion molecule (Dscam) (Levashina *et al.* 2001; Yu and Kanost 2002; Dong *et al.* 2006; Wang *et al.* 2019).

CTLs are Ca^{2+}-dependent carbohydrate-binding proteins possessing at least one carbohydrate-recognition domain (CRD) (Drickamer and Taylor 1993, 2015; Li *et al.* 2015). This protein superfamily contains more than 1 000 proteins (Brown *et al.* 2018). The typical C-type lectin-like domain (CTLD) is a double-loop structure containing anti-parallel *β*-sheets, two *α*-helices and two or three (long-form CTLD) conserved disulfides (Zelensky and Gready 2005). These conserved disulfides could stabilize the structure, and the second loop (long loop region) is related to the Ca^{2+}-dependent binding with carbohydrates (Zelensky and Gready 2003, 2005). In the vertebrate CTLD structure, based on Ca^{2+}-binding site 2, the EPN (Glu-Pro-Asn) motif determines the specific binding of mannose-type sugars, while the QPD (Gln-Pro-Asp) motif determines the specific binding of galactose-type sugars (Zelensky and Gready 2005; Brown *et al.* 2018).

Recently, many invertebrate CTLs have been characterized, with numerous novel motifs found in the invertebrate CTLs in addition to the conserved EPN and QPD motifs, such as QPN (Gln-Pro-Asn), EPD (Glu-Pro-Asp), NPS (Asn-Pro-Ser) and WND (Trp-Asn-Asp), along with several others (Wang and Wang 2013; Rao *et al.* 2015b). At present, the study of insect CTLs is mainly focused on *Drosophila*, *Manduca sexta*, mosquitoes (*Anopheles gambiae* and *Aedes aegypti*), *Bombyx mori* and *Helicoverpa armigera*. So far, 10, 34, 25, 39, 16, 9, 23, 34, 36, 25, 26 and 7 CTLs were identified in *Apis mellifera*, *Drosophila melanogaster*, *A. gambiae*, *A. aegypti*, *Tribolium castaneum*, *Nilaparvata lugens*, *B. mori*, *M. sexta*, *Ostrinia furnacalis*, *Spodoptera exigua*, *H. armigera* and *P. xylostella*, respectively (Xiong *et al.* 2015; Gasmi *et al.* 2018; Xia *et al.* 2018; Zhang *et al.* 2019; Song *et al.* 2020). The functions of insect CTLs found so far include cell adhesion, bacterial clearance, modulation of anti-fungal immunity, aggregation of hemocytes, enhancement of phagocytosis, encapsulation and melanization, stimulation of the proliferation of hemocytes, activation of prophenoloxidase (PPO), maintenance of intestinal microbiota homeostasis, promotion of virus entry into host cells, direct antibacterial or antiviral activity, and effects on the Cry toxicity and tissue regeneration (Ling *et al.* 2008; Batool *et al.* 2018; Xia *et al.* 2018; Zhang *et al.* 2019).

However, there are relatively few studies on *P. xylostella* CTLs. *Plutella xylostella* is a highly destructive pest of cruciferous crops worldwide (Furlong *et al.* 2013). It has developed resistance to almost all chemical insecticides that target it, as well as the biological insecticide *Bacillus thuringiensis* (Bt) (Sun *et al.* 2012; Furlong *et al.* 2013). Due to its rapid development of resistance, it is necessary to find novel and effective methods for the biological control of *P. xylostella*. As CTLs are involved in the identification and elimination of insect pathogens, the study of *P. xylostella* CTLs allows us to further understand how the insect interacts with microorganisms. In this study, a novel dual-CRD CTL (designated as PxIML) was identified from *P. xylostella*. The mRNA expression of *PxIML* at different developmental stages, tissues,

and in response to the stimulation by microorganisms were investigated. In addition, the functions of PAMPs recognition, microbe binding activity, microbial agglutination, encapsulation and phenoloxidase (PO) enhancement of PxIML were characterized. This study is significant for identifying the function of CTLs in *P. xylostella*, and more broadly improving our understanding of innate immunity in *P. xylostella*.

2. Materials and methods

2.1. Insect and microorganisms

The *P. xylostella* used in this study were reared at (25±2)°C, with 70–80% relative humidity and 16 h:8 h (light:dark). The larvae were fed on artificial diet (Lin *et al.* 2020) while adults were fed with 10% honey solution. Eggs were collected using egg cards smeared with powdered radish leaf.

Bacillus thuringiensis 8010 (Bt8010) strain was isolated from a cadaver of *Papilio polytes* (L.) larva in 1980 (Gao *et al.* 1986), and stored at the Key Laboratory of Biopesticide and Chemical Biology, Ministry of Education, Fujian Agriculture and Forestry University, Fuzhou, China. Bt8010 encodes nine Cry toxins (Cry1Na, Cry2Ab, Cry1Ea, Cry2Aa, Cry1If, Cry1Aa, Cry1Ai, Cry1Be-like and Cry1La-like) and two Vip toxins (Vip3Ad-like and Vip3Aa) based on its genome sequence (unpublished data). *Escherichia coli* BL21 (DE3) pG-Tf2 (TaKaRa Biotechnology, China), *E. coli* DH5α, *E.* coli BL21, *Enterobacter* sp. IAE5, *Serratia marcescens* IAE6, *Staphylococcus aureus* and *Pichia pastoris* strains were stored in the State Key Laboratory of Ecological Pest Control for Fujian and Taiwan Crops, Fujian Agricultural and Forestry University, Fuzhou, China. Bt8010 and *P. pastoris* were cultured at 30°C in Luria-Bertani (LB) and yeast extract peptone dextrose (YPD) media, respectively. The other bacteria were cultured at 37°C in LB.

2.2. Gene cloning

Total RNA of 4th instar larvae was extracted using Trizol® Reagent (Ambion, USA). The integrity and concentration of extracted RNA were detected by NanoDrop 2000 (Thermo Fisher Scientific, USA). The first strand cDNA was synthesized according to the GoScript™ Reverse Transcription System instructions (Promega, Madison, WI, USA). The *PxIML* coding sequence (CDS) was obtained from the DBM-DB (http://iae.fafu.edu.cn/DBM/). According to the sequence, the specific primers for cloning were designed by Primer Premier 6.0 (Appendix A). According to the manufacturer's instructions, PCR was carried out using Phanta® Max Super-Fidelity DNA Polymerase (Vazyme Biotech Co., Ltd., Nanjing, China), and the PCR condition was as follows: 95°C for 3 min; 95°C for 15 s, 58.5°C for 15 s and 72°C for 1 min (30 cycles); and 72°C for 5 min; then kept at 12°C. The PCR products were purified by Gel Extraction Kit (Omega Bio-tek, USA) and ligated into the pESI-Blunt simple vector (Yeasen Biotech Co., Ltd., Shanghai, China). The pESI-PxIML recombinant vector was transformed into *E. coli* DH5α, and then the bacterial liquid PCR was carried out with M13F and M13R. The positive clones were selected for DNA sequencing.

2.3. Sequence analysis

The amino acid sequence of PxIML was deduced by using the DNAMAN Software. The signal peptide and conserved domains were predicted by the SignalP 5.0 Server (http://www.cbs.dtu.dk/services/SignalP/) and SMART (http://smart.embl-heidelberg.de/smart/set_mode.cgi), respectively. The molecular weight and isoelectric point (pI) of PxIML were analyzed by ProtParam (http://web.expasy.org/protparam/).

2.4. Sequence alignments and phylogenetic analysis

The CTL sequences were selected from previous literature (Ao *et al.* 2007; Xiong *et al.* 2015; Batool *et al.* 2018; Xia *et al.* 2018; Bi *et al.* 2019; Zhang *et al.* 2019; Li *et al.* 2021), and from sequences with high similarity to PxIML in GenBank. The similarities of PxIML with other insect CTLs were compared by the protein–protein NCBI BLAST tool (http://blast.ncbi.nlm.nih.gov/Blast.cgi). Thirty-one CTLs from Lepidoptera (*H. armigera*: AFI47449.1, XP_021185772.1, XP_021200542.1 and XP_021194745.1; *S. exigua*: AQX37248.1; *Trichoplusia ni*: XP_026744357.1; *Galleria mellonella*: XP_026764354.1; *M. sexta*: XP_030038662.1 and AAF91316.3; *Bombyx mandarina*: XP_028037911.1; *B. mori*: NP_001091784.1, XP_004932809.1, XP_004931162.1, NP_001091747.1 and NP_001165397.1; *P. xylostella*: MT232645 and XP_011568909.1; *O. furnacalis*: MN453202.1 and XP_028164489.1; *Hyposmocoma kahamanoa*: XP_026329709.1; *Operophtera brumata*: KOB73959.1; *Spodoptera frugiperda*: XP_035436562.1; *Vanessa tameamea*: XP_026494963.1), Diptera (*A. gambiae*: XP_319374.4; *A. aegypti*: XP_001661644.2; *D. melanogaster*: NP_001014489.1 and NP_001014490.1) and Coleoptera (*T. castaneum*: NP_001164139.1 and NP_001164143.1; *Octodonta nipae*: QEL09433.1 and QEL09434.1) were selected for

multiple sequence alignment and phylogenetic analysis. The multiple sequence comparison was carried out using the ClustalW Multiple Alignment Program, and then decorated with Espript 3.0 (http://espript.ibcp.fr/ESPript/cgi-bin/ESPript.cgi). Based on the CTL amino acid sequences, the MEGA v.10.0.5 Program was used to build an unrooted phylogenetic tree by the neighbor-joining (NJ) algorithm (Kumar *et al.* 2018). All protein sequences were acquired from GenBank, and bootstrap resampling with 1 000 replicates was used for the verification of the phylogenetic tree. The NetNGlyc 1.0 (http://www.cbs.dtu.dk/services/NetNGlyc/) was used to predict N-glycosylation sites, and the NetOGlyc 4.0 (http://www.cbs.dtu.dk/services/NetOGlyc/) was used to predict O-glycosylation sites.

2.5. Predictions of protein structure model and ligand binding site

The 3D-structure model of PxIML was predicted by I-TASSER server (http://zhanglab.ccmb.med.umich.edu/I-TASSER/) (Yang *et al.* 2015). Protein-ligand binding sites were predicted by the COACH (Yang *et al.* 2013) and COFACTOR (Zhang *et al.* 2017) along with the I-TASSER server. The generated PDB files were then visualized with Pymol Molecular Graphics System.

2.6. Expression profiles of *PxIML*

To study the expression of *PxIML* in different developmental stages, total RNA was extracted from seven stages: eggs and 1st instar larvae covering the bottom of 1.5 mL tubes, 20 2nd instar larvae, five 3rd instar larvae, three 4th instar larvae, four pupae and three adults as a biological replicate. Each sample was repeated three times. To study the tissue expression of the *PxIML*, fat body, midgut, and hemocytes of *P. xylostella* 4th instar larvae were collected. The midgut and fat body were collected in RNA*later*™ RNA Stabilization Reagent (Qiagen, Germany), and the hemolymph was collected directly in the cell lysate. At least 30 4th instar larvae were dissected for each biological replicate. Each sample was repeated three times.

Next, to detect the expression of *PxIML* in early 4th instar larvae upon immune challenges, Bt8010, *S. marcescens* IAE6 and *P. pastoris* were used to infect the *P. xylostella*. Bt8010, *S. marcescens* IAE6 and *P. pastoris* were harvested by centrifugation at 9 000 r min^{-1} for 5 min, washed with sterilized water and suspended in sterilized water. The cell density (OD_{600}) was determined by T6 Ultraviolet-visible Spectrophotometer (Beijing Purkinje General Instrument Co., Ltd., Beijing, China). The sterilized artificial diet was prepared based on a previous study (Lin *et al.* 2020). The Bt8010, *S. marcescens* IAE6, *P. pastoris* or sterilized water (control) were immediately added to the sterilized artificial diet and mixed to a final density of OD_{600}=4.0 (Lin *et al.* 2020). The 4th instar larvae were starved for 4 h before being fed with the diet containing Bt8010, *S. marcescens* IAE6, *P. pastoris* or sterilized water, then the larvae were collected after being fed for 0, 6, 12, 18 and 24 h. At each of the five time points, the larvae with the highest expression were used for dissection and tissue expression analysis.

Total RNA was extracted using the RNAEastep® Super Total RNA Extraction Kit (Promega, Shanghai, China) and reverse transcribed using the FastKing RT Kit with gDNase (TIANGEN, Beijing, China). Quantitative real-time reverse transcription PCR (qRT-PCR) was performed using Go*Taq*® qPCR Master Mix (Promega, USA) on a CFX96 Touch™ Real-Time PCR Detection System (Bio-Rad, USA). The qRT-PCR condition was: 95°C for 3 min; 95°C for 20 s and 60°C for 30 s (40 cycles) and a melt curve from 60°C to 95°C in increments of 0.5°C for 5 s each. The cDNA samples were diluted with five concentration gradients (10×), and the standard curve of the gene was obtained. Gene expression levels were normalized to that of ribosomal protein L32 (GenBank ID: AB180441) (Chen *et al.* 2020) by the method of $2^{-\Delta\Delta C_T}$ (Zhang *et al.* 2009). Each biological replicate was performed in triplicate. Data were analyzed using one-way ANOVAs and *t*-tests in IBM SPSS Statistics 23 Software. The primers of the qRT-PCR are shown in Appendix A.

2.7. Expression and purification of recombinant PxIML

The cDNA sequence encoding the mature peptide of PxIML was amplified by the corresponding specific primers (Appendix A). *Nco*I endonuclease sites (CCATGG) in the *PxIML* sequence were mutated by a synonymous codon (ACAATGGAG). The 5′ end of the primers P7 and P8 contained *Nco*I and *Not*I endonuclease sites, respectively. The PCR reaction was first carried out using P8 and P9. The PCR reaction system is as described above, and the thermal cycling conditions were as follows: 95°C for 3 min; 95°C for 15 s, 63.5°C reduced by 0.5°C per cycle for 15 s and 72°C for 1 min (10 cycles); 95°C for 15 s, 58.5°C for 15 s and 72°C for 1 min (20 cycles), and 72°C for 5 min, then kept at 12°C. The second PCR was carried out using P7 and P10. The thermal cycling conditions were as follows: 95°C for 3 min; 95°C for 15 s, 61°C for 15 s and 72°C for 1 min (20 cycles); and 72°C

for 5 min, then kept at 12°C. After the two PCR products were purified and mixed as templates, the primers P7 and P8 were used for PCR. The PCR conditions were as follows: 95°C for 3 min; 95°C for 15 s, 57.5°C for 15 s and 72°C for 1 min (30 cycles); and 72°C for 5 min, then kept at 12°C. The PCR product and pET-28b vector were both digested by *Nco*I (NEB, USA) and *Not*I (TaKaRa, Japan). The ligation reaction was carried out using T4 DNA ligase (NEB, USA), then the expression vector (pET-28b-PxIML) with a 6×His-tag was obtained. Finally, the pET-28b-PxIML vector was transformed into *E. coli* BL21 (DE3) pG-Tf2 cells to yield the recombinant engineering bacteria. The recombinant engineering bacteria for PxIML production were cultured in 1 L of LB medium containing 50 μg mL^{-1} kanamycin, 20 μg mL^{-1} chloramphenicol, and 5 ng mL^{-1} tetracycline for 2.5 h at 37°C. The expression of recombinant PxIML (rPxIML) protein was induced by isopropyl-β-D-thiogalactopyranoside (IPTG, 0.5 mmol L^{-1}) at 16°C with shaking at 130 r min^{-1} and cultured for 24 h. The rPxIML was purified and concentrated according to Lin *et al.* (2020).

After the purified protein was concentrated, and the concentration of rPxIML protein was determined using the BCA Protein Quantification Kit (Yeasen Biotech Co., Ltd., Shanghai, China). SDS-PAGE and Western blotting based on the His-tag were used to analyze the expression of the rPxIML, and the purified protein was stored at –80°C.

2.8. Microbial binding assay

Six kinds of microorganisms: Gram-positive bacteria (*S. aureus* and Bt8010), Gram-negative bacteria (*E. coli* BL21, *Enterobacter* sp. IAE5, and *S. marcescens* IAE6), and fungi (*P. pastoris*), were used to test the binding activity of rPxIML. The *S. aureus*, *E. coli* BL21, *Enterobacter* sp. IAE5 and *S. marcescens* IAE6 were added to the liquid LB medium, and cultured at 37°C to a cell density of OD_{600}=1.0. The Bt8010 and *P. pastoris* were cultured in liquid LB and YPD media, respectively, at 30°C to a cell density of OD_{600}=1.0. After centrifugation at 8 000 r min^{-1} for 8 min, the microbial cells (200 μL) were resuspended in buffer B5 (20 mmol L^{-1} Tris-HCl, 150 mmol L^{-1} NaCl, 10% glycerol, pH 8.5, sterilized), and incubated with the purified rPxIML protein (7 μg) at room temperature. After incubation for 1 h, the supernatant was collected. The cells were washed with buffer B5 until no protein was detected in the supernatant using Coomassie Brilliant Blue G-250 (Beijing Solarbio Science & Technology Co., Ltd., Beijing, China), and the washing supernatant was collected. Finally, the binding protein was eluted on the oscillator using 7% SDS, and the eluting supernatant was collected. In this assay, 10 mmol L^{-1} $CaCl_2$ and 20 mmol L^{-1} EDTA were used to determine whether the rPxIML binding activity was dependent on Ca^{2+}. These collected supernatants were analyzed by Western blotting.

2.9. PAMPs binding assay

ELISA (enzyme-linked immunosorbent assay) was performed to examine the binding of rPxIML. A microtiter plate (Corning Costar, USA) was coated with 50 μL of 0.5 mg mL^{-1} lipopolysaccharides (LPS), peptidoglycan (PGN), D-galactose, mannan, N-acetyl-D-(+)-glucosamine and N-acetylneuraminic acid and air-dried at 37°C. After air-drying, in order to fix the carbohydrate, the 96-well plate was incubated at 60°C for 30 min, before each well was blocked with 200 μL of BSA (1 mg mL^{-1}, diluted in TBS) at 37°C for 2 h. After removing the blocking solution, a total of 50 μL TBS containing BSA (0.1 mg mL^{-1}) and rPxIML (0, 2, 4, 8 and 16 μg mL^{-1}) was added into each well and the plate was incubated at room temperature for 3 h. Those wells were rinsed four times with TBS and incubated with 100 μL of rabbit anti-His-tag antibody (Yeasen Biotech Co., Ltd., Shanghai, China) diluted 1:4 000 with BSA (0.1 mg mL^{-1}) in TBS at 37°C for 1 h. Next, the wells were washed four times with TBS, and incubated with 100 μL of HRP conjugated AffiniPure Goat anti-rabbit IgG (H+L) (Boster Biological Technology Co., Ltd., USA) diluted 1:10 000 with BSA (0.1 mg mL^{-1}) in TBS at 37°C for 1 h. After the wells had been washed again, 100 μL of TMB Single-Component Substrate solution (Solarbio, China) was added, with the reaction taking place at room temperature. When the color was moderate, 50 μL of ELISA stop solution (Solarbio, China) was immediately added into each well. After the reaction was terminated, the absorbance at 450 nm was monitored. Each of the protein concentration determinations was repeated in triplicate.

2.10. Microorganism agglutination assay

The agglutination activity of PxIML was detected according to established methodology (Yu *et al.* 2006). As previously described, six kinds of microorganisms (*S. aureus*, Bt8010, *E. coli* BL21, *Enterobacter* sp. IAE5, *S. marcescens* IAE6, and *P. pastoris*) at a cell density of OD_{600}=1.0 were suspended in buffer B5. The suspended microbes were incubated with 20 μL of FITC solution (10 mg mL^{-1} in DMSO) at room temperature in the dark for 1 h. After dyeing, the microbes were washed twice with buffer B5. The FITC-labelled microbes were suspended in 50 μL of buffer B5 containing 5 μg of rPxIML and incubated

in the dark for 45 min. Agglutination was observed by fluorescence microscopy (OLYMPUS IX51, Japan). To test whether the agglutination of rPxIML was Ca^{2+}-dependent, $CaCl_2$ (10 mmol L^{-1}) and EDTA (20 mmol L^{-1}) were added to the solution. BSA and buffer B5 were used as a control.

2.11. Encapsulation assay

Ni sepharose 6FF agarose beads (GE Healthcare, USA) were equilibrated in Tris-buffered saline (TBS; 20 mmol L^{-1} Tris-HCl, 150 mmol L^{-1} NaCl, pH 8.0, sterilized). The rPxIML was incubated with agarose beads at 4°C (excess proteins were detected in the remaining supernatant). The rPxIML-coated beads were washed and resuspended in TBS. To assess the encapsulation of hemocytes *in vitro*, 4th instar larvae of *P. xylostella* were washed with sterile water for 30 s, followed by 90 s with 75% alcohol, and then washed for a further 30 s with sterile water. The surface of 4th instar larvae was dried with aseptic filter paper, then the epidermis near the head was torn under an anatomical microscope to collect the fresh hemolymph. The fresh hemolymph was directly added to 200 μL Grace's medium containing 50 μg mL^{-1} tetracycline. The suspensions of 5 μL of rPxIML-coated or non-coated beads were incubated with 20 μL of hemolymph at room temperature for 2 h. A bead was defined as encapsulated when part of the surface, or the entire surface, was covered by a multilayer of hemocytes (Song *et al.* 2020). The encapsulation was observed under an Olympus BX43 microscope (Olympus, Japan).

2.12. Immunocytochemistry

Fresh hemolymph was drawn into an EP tube with anticoagulant. The hemocytes were collected by centrifugation at 500×g for 5 min at 4°C and suspended in TBS. The hemocyte suspension was dropped onto adhesive slides treated with lysine and allowed to settle for 2 h at room temperature. After settling, the hemocytes were fixed with 4% paraformaldehyde for 1 h and washed four times with TBS. Next, the hemocytes were blocked with 3% BSA at 37°C for 30 min and washed three times with TBS. After washing, the hemocytes were incubated with rPxIML (10 μg) at 4°C overnight and washed six times with TBS. Then, the hemocytes were incubated with the primary antibody rabbit anti-His-tag antibody (Yeasen Biotech Co., Ltd., Shanghai, China) at room temperature for 4 h. The primary antibody was diluted 1:1 000 in TBS containing 3% BSA. Subsequently, the hemocytes were washed six times, and incubated with goat anti-rabbit IgG conjugated with Alexa Fluor® 488 (Yeasen Biotech Co., Ltd., Shanghai, China) diluted 1:400 in TBS containing 3% BSA at 37°C in the dark for 1 h. After washing six times, the hemocytes were stained with 4′,6-diamidino-2-phenylindole dihydrochloride (DAPI) for 10 min. Finally, the samples were washed three times and sealed with 80% glycerol. In the experiment, TBS instead of His primary antibody and TBS instead of rPxIML were used as controls. The fluorescence signal was detected by a Leica TCS SP8 confocal microscope (Leica Microsystems, Germany).

2.13. PO activity assay

The PO activity was detected following a previously established methodology (Li *et al.* 2012). To obtain the plasma after centrifugation, hemolymph was collected from *P. xylostella* 4th instar larvae. First, four groups of mixtures were prepared; plasma group: the mixture contains 20 μL TBS, 20 μL diluted plasma and 0.4 μL $CaCl_2$; plasma+rPxIML group: the mixture contains 4 μL rPxIML, 16 μL TBS, 20 μL diluted plasma and 0.4 μL $CaCl_2$; plasma+IAE5 group: the mixture contains 4 μL heat-killed *Enterobacter* sp. IAE5, 16 μL TBS, 20 μL diluted plasma and 0.4 μL $CaCl_2$; plasma+IAE5+rPxIML group: the mixture contains 4 μL rPxIML, 4 μL heat-killed *Enterobacter* sp. IAE5, 12 μL TBS, 20 μL diluted plasma and 0.4 μL $CaCl_2$, with a final volume of 40.4 μL. After each mixture was incubated at room temperature for 10 min, 10 μL of this mixture was added into the 96-well plate. Subsequently, 200 μL of dopamine (2 mmol L^{-1}) was added to each well. The initial absorbance change at 490 nm was immediately measured using a Synergy™ H1 hybrid multimode microplate reader (BioTek, USA). One unit of enzyme activity was defined as an increase in absorbance (OD_{490}) of 0.001 min^{-1} (Jiang *et al.* 2003). Each treatment was performed in triplicate.

3. Results

3.1. Characterization of PxIML

The CTL gene was cloned from the diamondback moth genome and named as *PxIML* (GenBank accession number: MT232645). PxIML has an ORF of 969 bp encoding a 322 amino acid sequence (Appendix B). The first 23 amino acid residues in the N-terminal of PxIML were predicted to be a typical signal peptide. There are two CRD domains named in the order of CRD1 (residues 30–157) and CRD2 (residues 171–306). The mature PxIML protein has a theoretical molecular mass of 34.34 kDa and pI of 5.05. The 11 cysteine (Cys) residues in the mature amino acid sequence (positions Cys_{37},

Cys_{111}, Cys_{125} and Cys_{133} in CRD1; Cys_{146}; Cys_{162}, Cys_{179}, Cys_{260}, Cys_{274}, Cys_{278} and Cys_{282} in CRD2) might be involved in the formation of the disulfide bridge (Appendix B). The motifs of each CRD in the mature PxIML are different, which are EPN (Glu_{101}-Pro_{102}-Asn_{103}) in CRD1 and QPD (Gln_{251}-Pro_{252}-Asp_{253}) in CRD2.

3.2. Sequence alignment and phylogenetic analyses

The BLASTP analysis revealed significant similarity between PxIML and other insect CTLs. It shares 65.53% identity with OfIML10 (MN453202.1) from *O. furnacalis*, 60.19% with SeLL12 (AQX37247.1) and 59.94% with SeLL13 (AQX37248.1) from *S. exigua*. Multiple sequence alignment revealed PxIML contains ten conserved Cys residues and ligand binding sites (EPN and QPD) (Fig. 1). The ten highly conserved Cys residues (Cys_{37}, Cys_{111}, Cys_{125}, Cys_{133}, Cys_{146}, Cys_{162}, Cys_{179}, Cys_{260}, Cys_{274} and Cys_{282}) may generate at least four disulfide bonds. Glycosylation site analysis showed that each of the CRD may contain one N-glycosylation site (Asn_{84} and Asn_{194}), and there may also be two O-glycosylation sites (Ser_{25} and Thr_{225}) in the sequence.

Phylogenetic analysis showed that the selected CTLs are mainly divided into the single-CRD type and the dual-CRD type (immulectin). Interestingly, immulectins of Lepidoptera and two CTL-Xs (Haselectin and BmCTL-X) are clustered

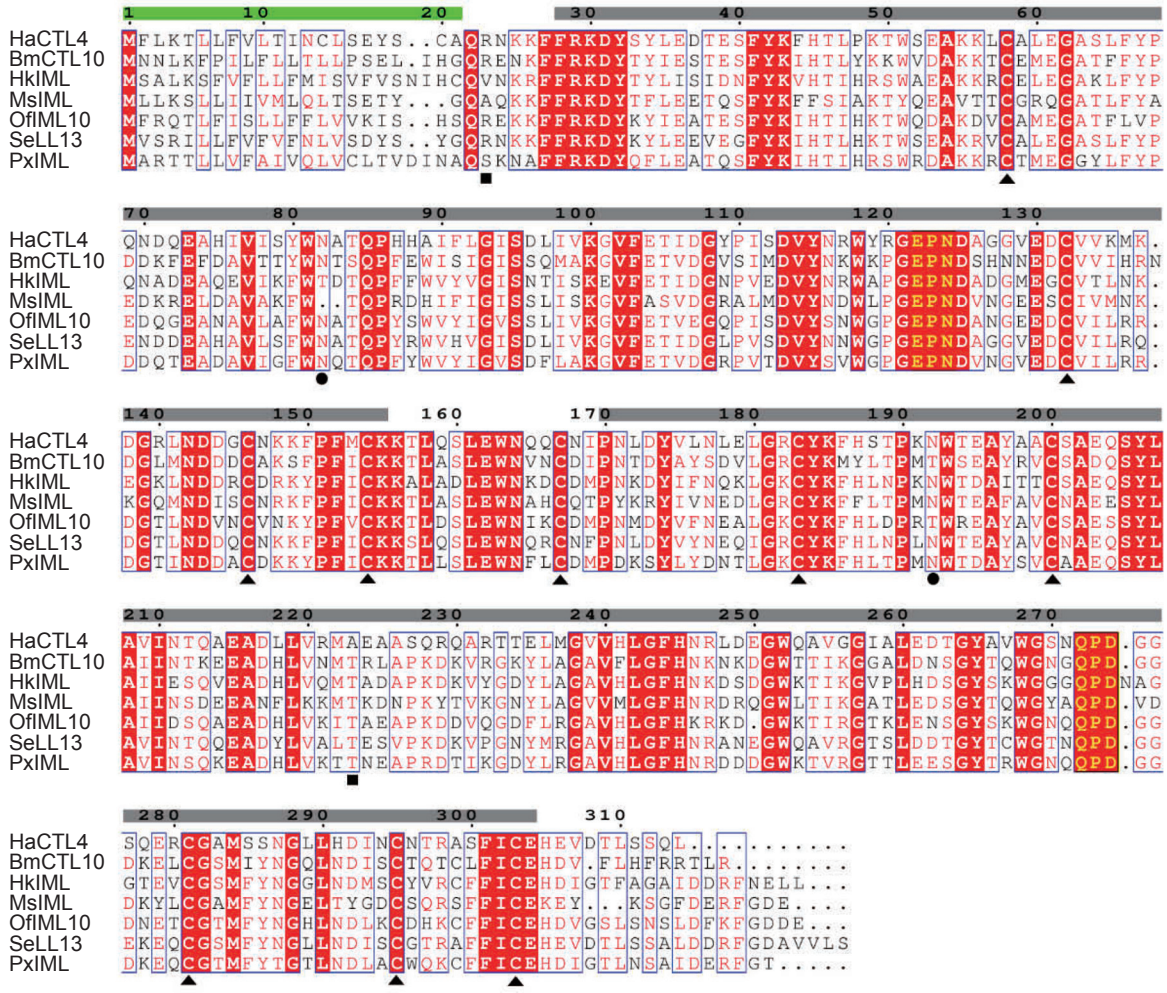

Fig. 1 Alignments of C-type lectins (CTLs) from *Plutella xylostella* and other insects. Signal peptides and CRDs are highlighted with green and grey lines above the sequences, respectively. Completely conserved residues are highlighted in red. EPN and QPD domains are highlighted by yellow. Conserved Cys residues are indicated by triangles. O-glycosylated and N-glycosylated sites are indicated by circles and squares, respectively. HaCTL4, *Helicoverpa armigera* CTL4 (AFI47449.1); BmCTL10, *Bombyx mori* CTL10 (NP_001091784.1); HkIML, *Hyposmocoma kahamanoa* immulectin (XP_026329709.1); MsIML, *Manduca sexta* immulectin (XP_030038662.1); OfIML10, *Ostrinia furnacalis* IML-10 (MN453202.1); SeLL13, *Spodoptera exigua* LL13 (AQX37248.1); PxIML, *P. xylostella* immulectin (MT232645).

into one sub-group, and the other two CTL-Xs (Hacontactin and Bmcontactin) are clustered with CTL-S group. In the CTL-S branch, Coleoptera appears closer to Lepidoptera than Diptera. In the branch of immulectin, *P. xylostella* PxIML and *O. furnacalis* IML-10 are the most homologous, and clustered into a sub-group (Appendix C).

3.3. Structure and ligand binding site analysis of PxIML

In the 3D structure of PxIML, CRD1 includes five *β*-stands and two *α*-helices, while CRD2 includes three *β*-stands, one patchy *α*-helix and two *α*-helices (Fig. 2). The I-TASSER server also used COACH to predict Ca^{2+}/Sugar binding sites based on the structural models. CRD1 has two potential CA (calcium) sites, a GQ4 (alpha-D-glucopyranosyl) site and a MAN (alpha-D-mannose) site, and CRD2 has a potential RAF (Raffinose) site (Fig. 2; Appendix D). The mannose-type MAN and GQ4 site contain amino acid residues (Glu_{101} and Asn_{103}) in the conserved EPN motif. The galactose-type RAF site contains amino acid residues (Gln_{251} and Asp_{253}) in the conserved QPD motif. The CA2 site includes interacting residues (Asp_{104} and Glu_{109}) with the MAN and GQ4 sites.

3.4. Expression profiles of *PxIML* in developmental stages and tissues

PxIML was found to be expressed in all stages of *P. xylostella*, but the expression varied with abundance and was the greatest in the 3rd instar larvae (Fig. 3-A, $F_{6, 14}$=74.39, P<0.05). No significant difference was observed between 4th instar larvae and adults (Fig. 3-A, P=0.902). The relative expression of *PxIML* in adults was significantly higher than in the egg, 1st instar larvae, 2nd instar larvae and pupae (Fig. 3-A, P<0.05).

The expression of *PxIML* in 4th instar larvae midgut, fat body and hemocytes were analyzed. *PxIML* was expressed in all three tissues of *P. xylostella*, and the expression abundance was the highest in the fat body (Fig. 3-B, $F_{2, 6}$=52.198, P<0.001). However, there was no significant difference observed between midgut and hemocytes (Fig. 3-B, P=0.999).

3.5. Expression profiles of *PxIML* under microbial challenge

The qRT-PCR results showed that the mRNA expression of *PxIML* was not significantly altered after infection with Bt8010 at 6 or 12 h (Fig. 4-A), but it was significantly

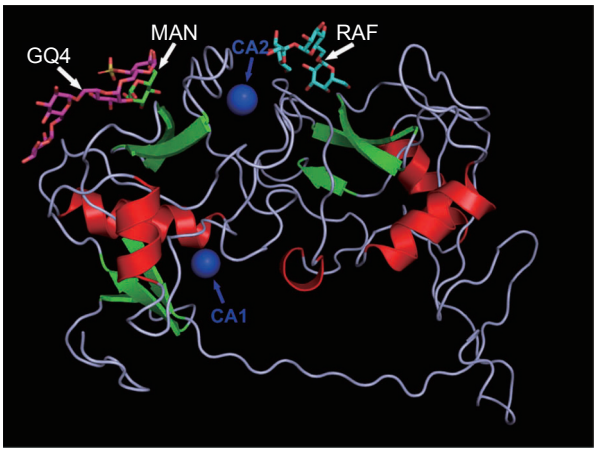

Fig. 2 Structural model of PxIML. The 3D structure of PxIML was built by the I-TASSER server. CA, Ca^{2+}; MAN, alpha-D-mannose; GQ4, alpha-D-glucopyranosyl; RAF, raffinose. The CA1 and CA2 are indicated by blue arrows. The MAN, RAF and GQ4 ligands are indicated by white arrows.

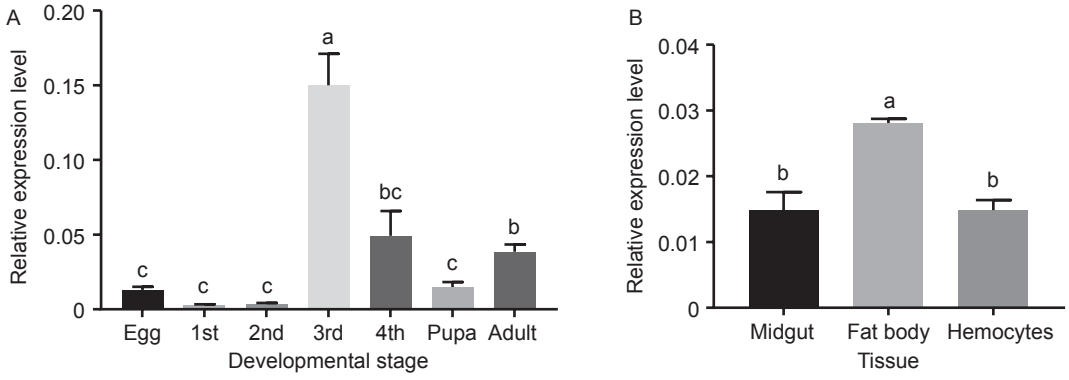

Fig. 3 Expression profiles of *PxIML* at different developmental stages (A) and in different tissues (B). 1st, 2nd, 3rd and 4th, indicate first, second, third and fourth instar larvae, respectively. The relative expression level is represented as mean±SD (n=3). Different letters indicate significant differences of expression among the different stages or tissues (one-way ANOVA followed by Games-Howell's test, P<0.05).

down-regulated after 18 h (Fig. 4-A, t_4=–3.366, P=0.028) and 24 h (Fig. 4-A, t_4=–4.481, P=0.011). The mRNA expression of *PxIML* was inhibited by Bt8010, however, mRNA expression of *PxIML* was significantly up-regulated under *S. marcescens* IAE6 infection at 12 h (Fig. 4-D, t_4=3.339, P=0.029) and 18 h (Fig. 4-D, t_4=4.979, P=0.008). Interestingly, the mRNA expression of *PxIML* was also significantly up-regulated under *P. pastoris* infection at 18 h (Fig. 4-G, t_4=3.035, P=0.039).

Tissue analysis revealed that the mRNA expression of *PxIML* was significantly down-regulated after infection with Bt8010 at 18 h, and the expression of *PxIML* in the fat body (Fig. 4-B, t_4=–4.947, P=0.008) and midgut (Fig. 4-C, t_4=–4.175, P=0.014) were significantly inhibited by Bt8010. The mRNA expression of *PxIML* in the fat body (Fig. 4-E, t_4=4.876, P=0.008) was significantly up-regulated at 18 h after infection with *S. marcescens* IAE6, but no significant difference was observed in the midgut (Fig. 4-F, t_4=0.213, P=0.842). The mRNA expression of *PxIML* in the fat body (Fig. 4-H, t_4=0.172, P=0.027) was significantly up-regulated at 18 h after infection with *P. pastoris*, but no significant difference was observed in the midgut (Fig. 4-I, t_4=0.174, P=0.870).

3.6. Production of the recombinant PxIML

The lysates of *E. coli* BL21 (DE3) pG-Tf2 cells with pET-28b-PxIML were collected and analyzed with SDS-PAGE. Western blotting analysis showed rPxIML exists both in the supernatant and precipitate (Appendix E). After purification, SDS-PAGE analysis showed high purity of rPxIML with a molecular mass of 35.8 kDa (Appendix E).

3.7. The binding capacity of rPxIML

In the presence of Ca^{2+} (10 mmol L^{-1}), rPxIML displayed strong binding ability to *E. coli* BL21, *Enterobacter* sp. IAE5, *S. marcescens* IAE6 and *S. aureus*, but it still had a weak binding ability in the absence of Ca^{2+} (Fig. 5-A). After adding EDTA (20 mmol L^{-1}) to inhibit Ca^{2+}, the binding ability of rPxIML to *Enterobacter* sp. IAE5, *S. marcescens* IAE6, *E. coli* BL21 and *S. aureus* were

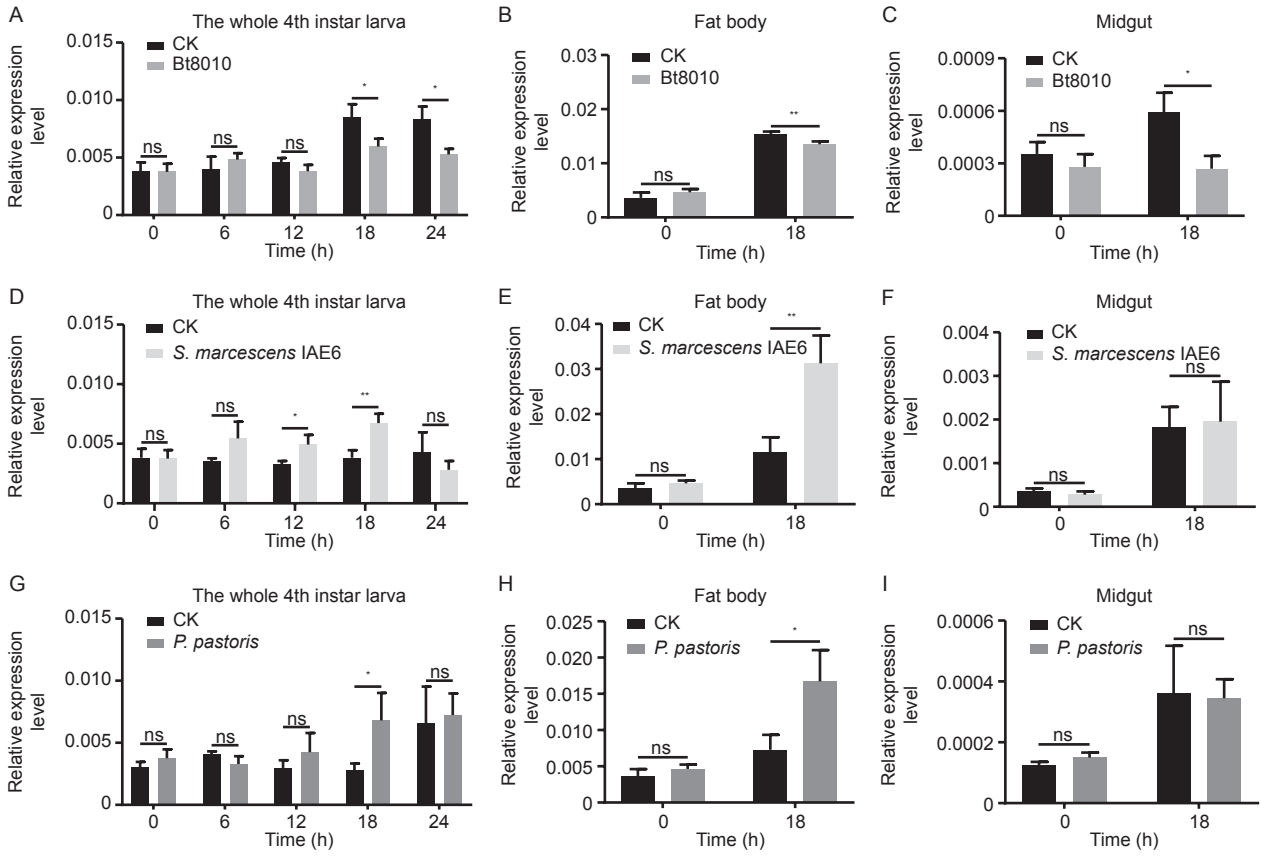

Fig. 4 Expression profiling of *PxIML* under microbial challenge. Expression profile analyses of *PxIML* in the whole 4th instar larva (A, D and G), fat body (B, E and H) and midgut (C, F and I) after *Bacillus thuringiensis* 8010, *Serratia marcescens* IAE6 and *Pichia pastoris* challenges, respectively. CK, sterilized water challenge. The relative expression level is represented as the mean±SD (n=3). The data were analyzed using the t-test of the independent samples. *, P<0.05; **, P<0.01; ns, no significant difference.

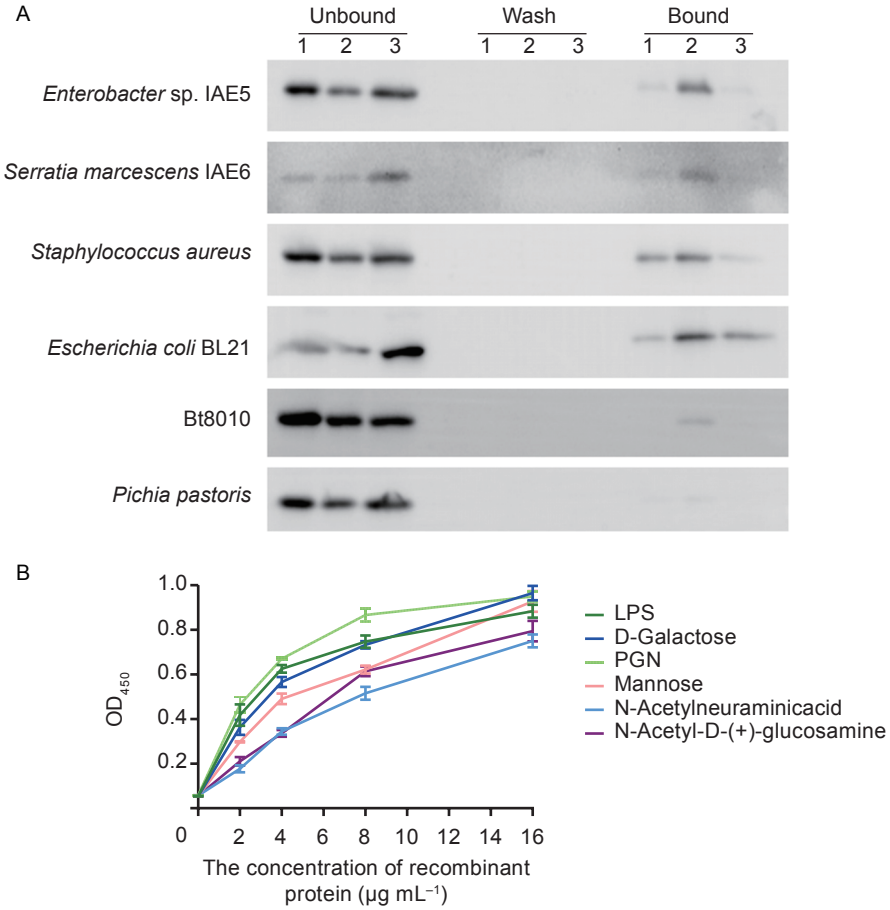

Fig. 5 Binding activity of the rPxIML to microbes and PAMPs. A, the microbe binding activity of rPxIML revealed by Western blotting. Unbound, unbound proteins in the supernatant after incubation of microbes and rPxIML; wash, the unbound proteins in the supernatant after incubation of microbes with rPxIML was removed and the supernatant collected after the microbes were washed four times; bound, bound proteins in the supernatant after elution; lane 1, microbes incubated with rPxIML; lane 2, microbes incubated with rPxIML and Ca^{2+} (10 mmol L^{-1}); lane 3, microbes incubated with rPxIML and Ca^{2+} (10 mmol L^{-1}) in the presence of EDTA (20 mmol L^{-1}). B, binding of rPxIML with the PAMPs. LPS, lipopolysaccharide; PGN, peptidoglycan. The rPxIML with concentrations of 0, 2, 4, 8 and 16 μg mL^{-1} were added to the wells fixed with PAMPs, then the binding results were detected by ELISA. The OD_{450} value is the mean±SE (n=3).

decreased. In addition, rPxIML weakly bound to Bt8010 and showed very limited binding to *P. pastoris* (Fig. 5-A).

In the PAMPs binding activity assay, when rPxIML bound to LPS, D-galactose, PGN, mannose, N-acetylneuraminic acid and N-acetyl-D-(+)-glucosamine, the absorbance at OD_{450} increased corresponding with the increase in rPxIML concentration (Fig. 5-B). Compared with the different PAMPs, the rPxIML exhibited the highest binding affinity to PGN.

3.8. Microorganism agglutination activity of rPxIML

In the presence of Ca^{2+} (10 mmol L^{-1}), rPxIML exhibited strong agglutination to *Enterobacter* sp. IAE5, *S. aureus* and Bt8010 and weak agglutination to *E. coli* BL21, while no agglutination to *S. marcescens* IAE6 or *P. pastoris* was observed (Fig. 6). The microorganism agglutination was not observed when the microbes were incubated in the buffer without Ca^{2+} or the buffer containing EDTA (20 mmol L^{-1}), indicating the agglutination activity of rPxIML was Ca^{2+}-dependent.

3.9. rPxIML promotes binding to hemocytes

The rPxIML-coated agarose beads were attached with more hemocytes than non-coated agarose beads, indicating that the rPxIML can promote the attachment of hemocytes to the beads (Fig. 7). At the same time, it can also promote melanization when the hemocytes attach to the beads (Fig. 7). Immunocytochemistry analysis suggested that rPxIML could bind to the surface molecules on *P. xylostella* hemocytes (Fig. 8).

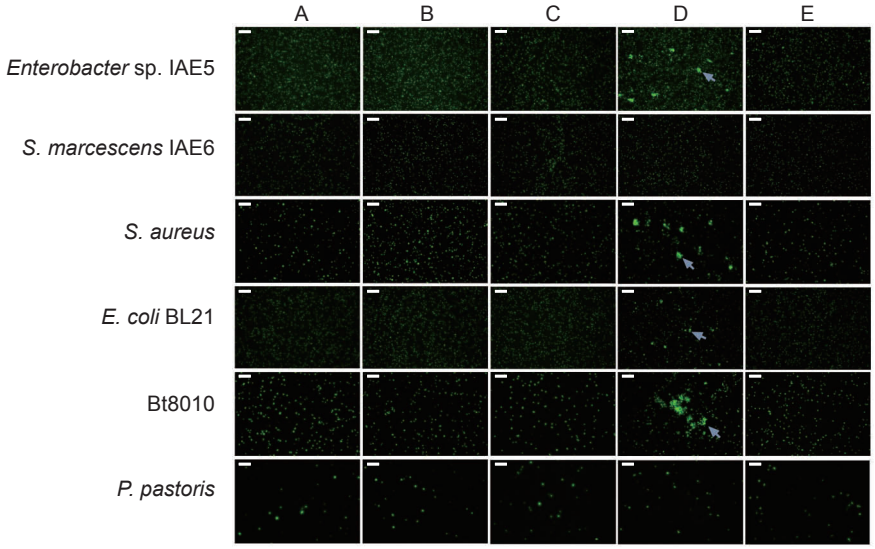

Fig. 6 Agglutination of microbes by rPxIML. A, FITC-labeled microbes incubated in buffer B5. B, FITC-labeled microbes incubated in buffer B5 with 5 μg BSA. C, FITC-labeled microbes incubated in buffer B5 with 5 μg rPxIML. D, FITC-labeled microbes incubated in buffer B5 with 5 μg rPxIML and Ca^{2+} (10 mmol L^{-1}). E, FITC-labeled microbes incubated in buffer B5 with 5 μg rPxIML and EDTA (20 mmol L^{-1}) in the presence of Ca^{2+} (10 mmol L^{-1}). In the presence of Ca^{2+} (10 mmol L^{-1}), rPxIML exhibited stronger agglutination to *Enterobacter* sp. IAE5, *Staphylococcus aureus* and *Bacillus thuringiensis* 8010, and weak agglutination to *Escherichia coli* BL21, while no agglutination to *Serratia marcescens* IAE6 or *Pichia pastoris* was observed. Arrows indicate agglutination. Scale bar is 50 μm.

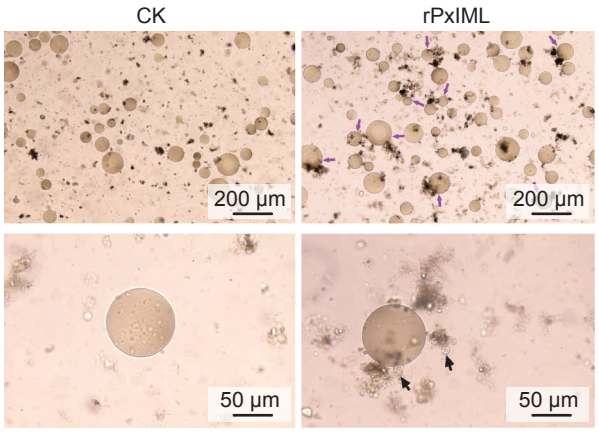

Fig. 7 PxIML promotes attachment of hemocytes to the beads. CK, the gel beads not coated with rPxIML. Encapsulation is not visible. CTL, the gel beads coated with rPxIML. The complete encapsulation is not found. The rPxIML promoted the attachment of hemocytes. Pink arrows indicate the attachment of hemocytes. Black arrows indicate hemocytes.

3.10. PO activation ability analysis

PO activity analysis revealed that heat-killed *Enterobacter* sp. IAE5 did not enhance the PO activity in *P. xylostella* plasma ($F_{3,8}$=15.879, P=0.126), however, the addition of rPxIML significantly enhanced the PO activity ($F_{3,8}$= 15.879, P=0.003) (Fig. 9).

4. Discussion

CTLs have been isolated from many invertebrate species due to interest in their important role in the insect innate immune response. In the present study, we identified the CTL from *P. xylostella*, PxIML. In insects, CTLs are divided into three groups: CTL-S, immulectin and CTL-X (Rao *et al.* 2015a; Xia *et al.* 2018). Immulectin contains two tandem CRD, which are mainly found in Lepidoptera species (Yu and Kanost 2001; Rao *et al.* 2015b). The number of different Lepidoptera immulectins varies greatly, such as *B. mori* with 6 (Rao *et al.* 2015b), *M. sexta* with 19 (Rao *et al.* 2015a) and *O. furnacalis* with 15 (Song *et al.* 2020). However, there is only one immulectin in *P. xylostella*. Although *P. xylostella* contains fewer CTL than other species, βGRP is greatly expanded in *P. xylostella* (Xia *et al.* 2015). We still do not know why this phenomenon occurs in *P. xylostella*, whether it is related to species specificity, whether the function of the CTL gene in *P. xylostella* is supplemented by other pattern recognition receptors, such as βGRP, or if the CTL of *P. xylostella* has more diverse functions. All these possibilities require further study. For insect immulectins, including PxIML, the N-terminal CRD1 is a short-form CRD, whereas the C-terminal CRD2 is a long-form CRD (Yu and Kanost 2000).

To verify the immune function of PxIML in *P. xylostella*,

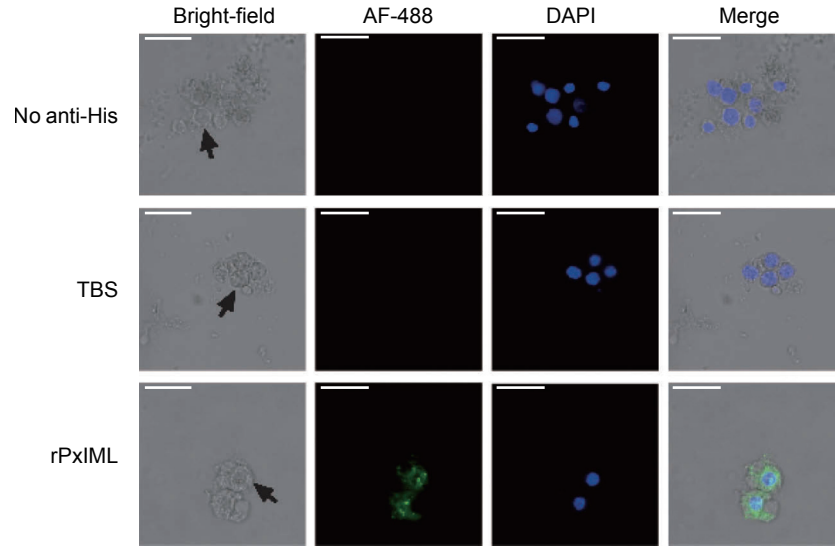

Fig. 8 Binding activity of rPxIML to hemocytes. No anti-His, the treatment without anti-His; TBS, the treatment using TBS; rPxIML, the treatment with rPxIML. Arrows indicate hemocytes. Scale bar is 20 μm.

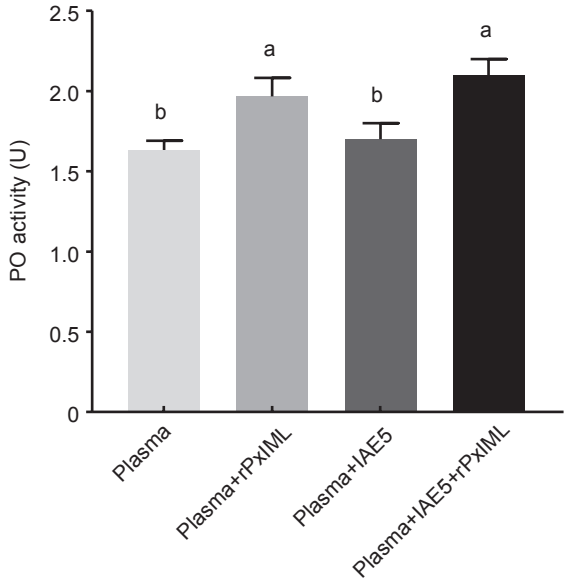

Fig. 9 Effect of rPxIML on phenoloxidase (PO) activity. Plasma, plasma isolated from *Plutella xylostella*; plasma+rPxIML, rPxIML was added to the plasma isolated from *P. xylostella*; plasma+IAE5, heat-killed *Enterobacter* sp. IAE5 was added to the plasma isolated from *P. xylostella*; plasma+IAE5+rPxIML, rPxIML and heat-killed *Enterobacter* sp. IAE5 were added to the plasma isolated from *P. xylostella*. PO activity is represented as mean±SD (n=3). The different letter labels indicate significant differences (P<0.05) between treatments.

its mRNA expression levels were first examined in seven developmental stages and three tissues. We found that *PxIML* mRNA was detected in all developmental stages of healthy *P. xylostella*, but the mRNA expression of *PxIML* was the highest in 3rd instar larvae, followed by 4th instar larvae, implying that PxIML may play a significant role at the larval stage. The peak feeding period of *P. xylostella* is in 4th instar, when it consumes around 83% of its total food intake (Lu and Chen 1986). Consequently, the pathogens it faces may be more complex. For this reason, we considered the detection of tissue expression during this development period to be particularly valuable. Tissue expression analysis showed that expression of *PxIML* was the highest in the fat body, which is similar to *BmLBP* and *BmIML* previously observed in *B. mori* (Takase *et al.* 2009), *IML-1* and *IML-2* from *M. sexta* (Yu and Kanost 2000) and *IML-10* from *O. furnacalis* (Song *et al.* 2020). The study of microbial infection indicated that the mRNA expression of *PxIML* in 4th instar larvae whole body and fat body was significantly up-regulated when infected with *S. marcescens* IAE6 and *P. pastoris*, results similar to those observed previously for the *Ha-lectin* in *H. armigera* (Chai *et al.* 2008), *CTL4* and *CTLMA2* in *A. gambiae* (Schnitger *et al.* 2009) and *PtCLec1* in *Portunus trituberculatus* (Su *et al.* 2020). The up-regulation of *PxIML* expression after infection with *S. marcescens* IAE6 and *P. pastoris* may be due to the fact that PxIML participates in the immune defense against these two microbes. On the contrary, the mRNA expression of *PxIML* was significantly down-regulated in the whole body, fat body and midgut when 4th instar larvae of *P. xylostella* were infected with Bt8010. This is similar to the down-regulation of the overall expression trend of *T. castaneum* TcCTL6 after PGN injection. The bacteria may achieve a certain protection against the

host immune system attack by down-regulating TcCTL6 (Bi *et al.* 2019). However, determining whether the inhibition of PxIML expression was caused by the Bt8010 strain itself, the toxin released from Bt8010, or even other proteins released by Bt8010, still needs further study. This result suggests that Bt8010 may prevent the activation of the downstream immune response, further protecting it from the *P. xylostella* immune system.

Generally, CTLs contain at least one CRD with the EPN motif or QPD motif (Zheng *et al.* 2020). Notably, the variation motif was found in other immulectins, for example, BmLBP with EPD and EPS motifs in *B. mori* (Takase *et al.* 2009), IML-1 with a QPR motif and IML-8 with APN in *M. sexta* (Yu and Kanost 2000; Rao *et al.* 2015a). In general, the extensive binding activity of insect CTLs with tandem CRD to carbohydrates on the pathogen surface may be higher than that of single-CRD CTLs (Yu and Kanost 2000). In *P. xylostella*, CRD1 of PxIML was found with an EPN motif, and CRD2 with a QPD motif. Based on the 3D structure, the PxIML may bind to mannose and galactose. Fc-Lec2 of *Fenneropenaeus chinensis* contains CRD1 with QPD and CRD2 with EPN, and CRD1 can bind to D-galactose, while CRD2 binds to D-mannose, therefore, their functions may be complementary (Zhang *et al.* 2009). Interestingly, our experiment revealed that the rPxIML can bind to D-galactose and mannose, thus, we predict that the functions of CRD1 and CRD2 of PxIML may also complement each other to extend the binding range. The rPxIML can directly bind to LPS, PGN, D-galactose, mannose, N-acetyl-D-(+)-glucosamine and N-acetylneuraminic acid in the absence of Ca^{2+}, which is consistent with the results of Fc-Lec2 in *F. chinensis* (Zhang *et al.* 2009), IML-2 in *M. sexta* (Yu and Ma 2006) and CTL-S2 in *B. mori* (Shahzad *et al.* 2017). Based on the microbial binding assay, we found that PxIML could bind to a variety of Gram-negative and Gram-positive bacteria, but not the fungus *P. pastoris*. Although Ca^{2+} enhanced the binding activity of rPxIML to bacteria, it was not essential. This is consistent with results seen for IML-2 in *M. sexta* (Yu and Ma 2006), EsLecH in *Eriocheir sinensis* (Zhu *et al.* 2016), DjCTL in *Dugesia japonica* (Gao *et al.* 2017) and TcCTL3 in *T. castaneum* (Bi *et al.* 2020).

An agglutination reaction occurs when C-type lectins bind to microorganisms, which facilitates the clearing of invaders by the host defense system. In invertebrates, the agglutination activity of C-type lectins is dependent on Ca^{2+}. The Ca^{2+} may promote the formation of lectin oligomers or compact structures (Bi *et al.* 2020). Our study has revealed that rPxIML exhibited stronger agglutination activities towards *Enterobacter* sp. IAE5, *S. aureus*, and Bt8010, but weak agglutination activity toward *E. coli* BL21 with Ca^{2+}. In *M. sexta*, IML-2 may contain a Ca^{2+}-binding site which is different from the carbohydrate binding sites and is required for agglutination activity (Yu and Ma 2006). Thus, there may be Ca^{2+} binding sites which differ from the EPN and QPD motifs related to the agglutination activity in PxIML. In addition, there was no agglutination to *S. marcescens* IAE6 or *P. pastoris* even in a Ca^{2+} environment, however, although the rPxIML could not agglutinate *S. marcescens* IAE6, it could bind to *S. marcescens* IAE6. We speculated that PxIML may only recognize *S. marcescens* IAE6 but lack the subsequent direct agglutination and scavenging function. Another interesting finding is that PxIML can respond to fungal *P. pastoris* stimulation without being able to bind or agglutinate it. The immune response of PxIML to fungi may be different from TcCTL3, TcCTL5 and TcCTL6 of *T. castaneum* (Bi *et al.* 2019, 2020; Li *et al.* 2020) and PtCLec1 of *P. tritubercula*tus (Su *et al.* 2020). The reason for this difference may be that PxIML cannot directly participate in the recognition of *P. pastoris*, but only through other upstream pattern recognition receptors, and then the signal is transmitted to the PxIML, resulting in changes in the expression of PxIML. For example, in the Toll pathway, Toll receptors usually do not directly bind to pathogens, but instead, the pathogens are recognized by other upstream pattern recognition receptors, such as PGRP or βGRP, and then gradually the signal is transmitted to the Spätzle (SPZ) and Toll receptors (Gobert *et al.* 2003; Huang *et al.* 2015; Xia *et al.* 2015). Of course, whether such a pathway exists in PxIML still needs further verification. Moreover, as only one kind of fungus was used in this experiment, these conclusions require further verification by exploring the interactions with more fungal species.

Encapsulation is an immune clearance process in which hemocytes attach to large nonself-particles. In insects, it is accompanied by melanization through activation of the PPO system (Huang *et al.* 2017). In *O. furnacalis*, IML-10 can bind to the hemocytes to promote their aggregation and further improve their encapsulation capacity (Song *et al.* 2020). Previous studies have shown that integrin β1 is involved in modulating hemocytic encapsulation in *H. armigera* (Xu *et al.* 2012), Haβ-integrin may act as a HaCTL3 receptor in the process of hemocytic encapsulation, and glycosylation modification may be the key to the HaCTL3-Haβ-integrin interaction (Wang *et al.* 2017). In the present study, rPxIML was found to bind to the surface of hemocytes and promote the attachment of hemocytes. At the same time, it also promoted the occurrence of melanization. However, complete encapsulation was not found, which is different from *O. furnacalis* IML-10, *M. sexta* IMLs (IML-

1, 2, 3) and *H. armigera* HaCTL3 (Ling and Yu 2006; Wang *et al*. 2017; Song *et al*. 2020). It is not known whether the low efficiency of the encapsulation function of rPxIML is due to the lack of a receptor, such as effective integrin, or a lack of glycosylation modification in the *in vitro* system, or by another unidentified mechanism. Further study is still needed to elucidate the exact cause of the low encapsulation efficiency for rPxIML. It is also worth noting that as rPxIML was expressed and purified from *E. coli*, we cannot rule out the possible effect of host bacterial endotoxin participation in the PO activation. We suggest that future studies could utilize insect cell expression, or more rigorous control trials which are designed to confirm the function of the protein and identify whether PxIML is the only factor promoting melanization.

5. Conclusion

A novel C-type lectin PxIML containing a dual-CRD with typical motifs of EPN and QPD was cloned and characterized from *P. xylostella*. When *P. xylostella* was infected by *S. marcescens* IAE6 or *P. pastoris*, PxIML could participate in the immune defense mechanism against them, however, Bt8010 may evade the attack from the immune system by inhibiting PxIML. PxIML not only has binding and agglutinating activities for various bacteria, but it also promotes melanization and PO activity. These results indicate that PxIML can be used as a PRR which participates in cellular and humoral immunity of *P. xylostella*. This study provides evidence for the function of CTLs in the interactions of *P. xylostella* and its associated pathogens. Additionally, this study provides a new potential focus for biocontrol technologies targeting *P. xylostella*.

Acknowledgements

This research was supported by the project of the National Key R&D Program of China (2017YFE0122000), the National Natural Science Foundation of China (31871968), and the Natural Science Foundation of Fujian Province, China (2018J01614).

Declaration of competing interest

The authors declare that they have no conflict of interest.

Appendices associated with this paper are available on http://www.ChinaAgriSci.com/V2/En/appendix.htm

References

Ao J, Ling E, Yu X Q. 2007. *Drosophila* C-type lectins enhance cellular encapsulation. *Molecular Immunology*, **44**, 2541–2548.

Batool K, Alam I, Zhao G, Wang J, Xu J, Yu X, Huang E, Guan X, Zhang L. 2018. C-type lectin-20 interacts with ALP1 receptor to reduce Cry toxicity in *Aedes aegypti*. *Toxins* (Basel), **10**, 390.

Bi J, Feng F, Li J, Mao J, Ning M, Song X, Xie J, Tang J, Li B. 2019. A C-type lectin with a single carbohydrate-recognition domain involved in the innate immune response of *Tribolium castaneum*. *Insect Molecular Biology*, **28**, 649–661.

Bi J, Ning M, Li J, Zhang P, Wang L, Xu S, Zhong Y, Wang Z, Song Q, Li B. 2020. A C-type lectin with dual-CRD from *Tribolium castaneum* is induced in response to bacterial challenge. *Pest Management Science*, **76**, 3965–3974.

Brown G D, Willment J A, Whitehead L. 2018. C-type lectins in immunity and homeostasis. *Nature Reviews*: *Immunology*, **18**, 374–389.

Chai L Q, Tian Y Y, Yang D T, Wang J X, Zhao X F. 2008. Molecular cloning and characterization of a C-type lectin from the cotton bollworm, *Helicoverpa armigera*. *Developmental and Comparative Immunology*, **32**, 71–83.

Chen W, Dong Y, Saqib H S A, Vasseur L, Zhou W, Zheng L, Lai Y, Ma X, Lin L, Xu X, Bai J, He W, You M. 2020. Functions of duplicated glucosinolate sulfatases in the development and host adaptation of *Plutella xylostella*. *Insect Biochemistry and Molecular Biology*, **119**, 103316.

Dong Y, Aguilar R, Xi Z, Warr E, Mongin E, Dimopoulos G. 2006. *Anopheles gambiae* immune responses to human and rodent *Plasmodium parasite* species. *PLoS Pathogens*, **2**, e52.

Drickamer K, Taylor M E. 1993. Biology of animal lectins. *Annual Review of Cell and Developmental Biology*, **9**, 237–264.

Drickamer K, Taylor M E. 2015. Recent insights into structures and functions of C-type lectins in the immune system. *Current Opinion in Structural Biology*, **34**, 26–34.

Furlong M J, Wright D J, Dosdall L M. 2013. Diamondback moth ecology and management: Problems, progress, and prospects. *Annual Review of Entomology*, **58**, 517–541.

Gao L, Han Y, Deng H, Hu W, Zhen H, Li N, Qin N, Yan M, Wu W, Liu B, Zhao B, Pang Q. 2017. The role of a novel C-type lectin-like protein from planarian in innate immunity and regeneration. *Developmental and Comparative Immunology*, **67**, 413–426.

Gao R X, Lin G X, Guan X, Luo Y F. 1986. Studies on the new strain of *Bacillus thuringensis* var. Kurstaki 8010. *Journal of Fujian Agricultural College*, **15**, 1–10. (in Chinese)

Gasmi L, Jakubowska A K, Ferré J, Ogliastro M, Herrero S. 2018. Characterization of two groups of *Spodoptera exigua* Hübner (Lepidoptera: Noctuidae) C-type lectins and insights into their role in defense against the densovirus JcDV. *Archives of Insect Biochemistry and Physiology*, **97**, e21432.

Gobert V, Gottar M, Matskevich A A, Rutschmann S, Royet J, Belvin M, Hoffmann J A, Ferrandon D. 2003. Dual activation of the *Drosophila* toll pathway by two pattern recognition receptors. *Science*, **302**, 2126–2130.

Huang M, Mu C, Wu Y, Ye F, Wang D, Sun C, Lv Z, Han B, Wang C, Xu X W. 2017. The functional characterization and comparison of two single CRD containing C-type lectins with novel and typical key motifs from *Portunus trituberculatus*. *Fish and Shellfish Immunology*, **70**, 398–407.

Huang W, Xu X, Freed S, Zheng Z, Wang S, Ren S, Jin F. 2015. Molecular cloning and characterization of a β-1,3-glucan recognition protein from *Plutella xylostella* (L.). *New Biotechnology*, **32**, 290–299.

Jiang H, Wang Y, Yu X Q, Kanost M R. 2003. Prophenoloxidase-activating proteinase-2 from hemolymph of *Manduca sexta*. A bacteria-inducible serine proteinase containing two clip domains. *Journal of Biological Chemistry*, **278**, 3552–3561.

Kumar S, Stecher G, Li M, Knyaz C, Tamura K. 2018. MEGA X: Molecular evolutionary genetics analysis across computing platforms. *Molecular Biology and Evolution*, **35**, 1547–1549.

Lavine M D, Strand M R. 2002. Insect hemocytes and their role in immunity. *Insect Biochemistry and Molecular Biology*, **32**, 1295–1309.

Levashina E A, Moita L F, Blandin S, Vriend G, Lagueux M, Kafatos F C. 2001. Conserved role of a complement-like protein in phagocytosis revealed by dsRNA knockout in cultured cells of the mosquito, *Anopheles gambiae*. *Cell*, **104**, 709–718.

Li H, Zhang H, Jiang S, Wang W, Xin L, Wang H, Wang L, Song L. 2015. A single-CRD C-type lectin from oyster *Crassostrea gigas* mediates immune recognition and pathogen elimination with a potential role in the activation of complement system. *Fish and Shellfish Immunology*, **44**, 566–575.

Li J, Bi J, Zhang P, Wang Z, Zhong Y, Xu S, Wang L, Li B. 2021. Functions of a C-type lectin with a single carbohydrate-recognition domain in the innate immunity and movement of the red flour beetle, *Tribolium castaneum*. *Insect Molecular Biology*, **30**, 90–101.

Li X, Ma M, Liu F, Chen Y, Lu A, Ling Q Z, Li J, Beerntsen B T, Yu X Q, Liu C, Ling E. 2012. Properties of *Drosophila melanogaster* prophenoloxidases expressed in *Escherichia coli*. *Developmental and Comparative Immunology*, **36**, 648–656.

Lin J, Yu X Q, Wang Q, Tao X, Li J, Zhang S, Xia X, You M. 2020. Immune responses to *Bacillus thuringiensis* in the midgut of the diamondback moth, *Plutella xylostella*. *Developmental and Comparative Immunology*, **107**, 103661.

Ling E, Ao J, Yu X Q. 2008. Nuclear translocation of immulectin-3 stimulates hemocyte proliferation. *Molecular Immunology*, **45**, 2598–2606.

Ling E, Yu X Q. 2006. Cellular encapsulation and melanization are enhanced by immulectins, pattern recognition receptors from the tobacco hornworm *Manduca sexta*. *Developmental and Comparative Immunology*, **30**, 289–299.

Lowenberger C A, Smartt C T, Bulet P, Ferdig M T, Severson D W, Hoffmann J A, Christensen B M. 1999. Insect immunity: molecular cloning, expression, and characterization of cDNAs and genomic DNA encoding three isoforms of insect defensin in *Aedes aegypti*. *Insect Molecular Biology*, **8**, 107–118.

Lu Z Q, Chen L F. 1986. Studies on *Plutella xylostella* in Yangzhou region. *Jiangsu Agricultural Sciences*, **2**, 21–23. (in Chinese)

Rao X J, Cao X, He Y, Hu Y, Zhang X, Chen Y R, Blissard G, Kanost M R, Yu X Q, Jiang H. 2015a. Structural features, evolutionary relationships, and transcriptional regulation of C-type lectin-domain proteins in *Manduca sexta*. *Insect Biochemistry and Molecular Biology*, **62**, 75–85.

Rao X J, Shahzad T, Liu S, Wu P, He Y T, Sun W J, Fan X Y, Yang Y F, Shi Q, Yu X Q. 2015b. Identification of C-type lectin-domain proteins (CTLDPs) in silkworm *Bombyx mori*. *Developmental and Comparative Immunology*, **53**, 328–338.

Schnitger A K, Yassine H, Kafatos F C, Osta M A. 2009. Two C-type lectins cooperate to defend *Anopheles gambiae* against Gram-negative bacteria. *Journal of Biological Chemistry*, **284**, 17616–17624.

Shahzad T, Zhan M Y, Yang P J, Yu X Q, Rao X J. 2017. Molecular cloning and analysis of a C-type lectin from silkworm *Bombyx mori*. *Archives of Insect Biochemistry and Physiology*, **95**, e21391.

Song Z K, Tian M L, Dong Y P, Ren C B, Du Y, Hu J. 2020. The C-type lectin IML-10 promotes hemocytic encapsulation by enhancing aggregation of hemocytes in the Asian corn borer *Ostrinia furnacalis*. *Insect Biochemistry and Molecular Biology*, **118**, 103314.

Su Y, Liu Y, Gao F, Cui Z. 2020. A novel C-type lectin with a YPD motif from *Portunus trituberculatus* (PtCLec1) mediating pathogen recognition and opsonization. *Developmental and Comparative Immunology*, **106**, 103609.

Sullivan J T, Belloir J A. 2014. Activation of an innate immune response in the schistosome-transmitting snail *Biomphalaria glabrata* by specific bacterial PAMPs. *Developmental and Comparative Immunology*, **42**, 256–260.

Sun J, Liang P, Gao X. 2012. Cross-resistance patterns and fitness in fufenozide-resistant diamondback moth, *Plutella xylostella* (Lepidoptera: Plutellidae). *Pest Management Science*, **68**, 285–289.

Takase H, Watanabe A, Yoshizawa Y, Kitami M, Sato R. 2009. Identification and comparative analysis of three novel C-type lectins from the silkworm with functional implications in pathogen recognition. *Developmental and Comparative Immunology*, **33**, 789–800.

Wang P, Zhuo X R, Tang L, Liu X S, Wang Y F, Wang G X, Yu X Q, Wang J L. 2017. C-type lectin interacting with β-integrin enhances hemocytic encapsulation in the cotton bollworm, *Helicoverpa armigera*. *Insect Biochemistry and Molecular Biology*, **86**, 29–40.

Wang X, Zhang Y, Zhang R, Zhang J. 2019. The diversity of pattern recognition receptors (PRRs) involved with insect defense against pathogens. *Current Opinion in Insect*

Science, **33**, 105–110.

Wang X W, Wang J X. 2013. Diversity and multiple functions of lectins in shrimp immunity. *Developmental and Comparative Immunology*, **39**, 27–38.

Xia X, You M, Rao X J, Yu X Q. 2018. Insect C-type lectins in innate immunity. *Developmental and Comparative Immunology*, **83**, 70–79.

Xia X, Yu L, Xue M, Yu X, Vasseur L, Gurr G M, Baxter S W, Lin H, Lin J, You M. 2015. Genome-wide characterization and expression profiling of immune genes in the diamondback moth, *Plutella xylostella* (L.). *Scientific Reports*, **5**, 9877.

Xiong G H, Xing L S, Lin Z, Saha T T, Wang C, Jiang H, Zou Z. 2015. High throughput profiling of the cotton bollworm *Helicoverpa armigera* immunotranscriptome during the fungal and bacterial infections. *BMC Genomics*, **16**, 321.

Xu Q, Yu X, Liu J, Zhao H, Wang P, Hu S, Chen J, Zhang W, Hu J. 2012. *Ostrinia furnacalis* integrin β1 may be involved in polymerization of actin to modulate spreading and encapsulation of plasmatocytes. *Developmental and Comparative Immunology*, **37**, 438–445.

Yang J, Roy A, Zhang Y. 2013. Protein-ligand binding site recognition using complementary binding-specific substructure comparison and sequence profile alignment. *Bioinformatics*, **29**, 2588–2595.

Yang J, Yan R, Roy A, Xu D, Poisson J, Zhang Y. 2015. The I-TASSER Suite: protein structure and function prediction. *Nature Methods*, **12**, 7–8.

Yu X Q, Kanost M R. 2000. Immulectin-2, a lipopolysaccharide-specific lectin from an insect, *Manduca sexta*, is induced in response to gram-negative bacteria. *Journal of Biological Chemistry*, **275**, 37373–37381.

Yu X Q, Kanost M R. 2001. A family of C-type lectins in *Manduca sexta*. *Advances in Experimental Medicine and Biology*, **484**, 191–194.

Yu X Q, Kanost M R. 2002. Binding of hemolin to bacterial lipopolysaccharide and lipoteichoic acid. An immunoglobulin superfamily member from insects as a pattern-recognition receptor. *European Journal of Biochemistry*, **269**, 1827–1834.

Yu X Q, Ling E, Tracy M E, Zhu Y. 2006. Immulectin-4 from the tobacco hornworm *Manduca sexta* binds to lipopolysaccharide and lipoteichoic acid. *Insect Molecular Biology*, **15**, 119–128.

Yu X Q, Ma Y. 2006. Calcium is not required for immulectin-2 binding, but protects the protein from proteinase digestion. *Insect Biochemistry and Molecular Biology*, **36**, 505–516.

Zelensky A N, Gready J E. 2003. Comparative analysis of structural properties of the C-type-lectin-like domain (CTLD). *Proteins*, **52**, 466–477.

Zelensky A N, Gready J E. 2005. The C-type lectin-like domain superfamily. *FEBS Journal*, **272**, 6179–6217.

Zhang C, Freddolino P L, Zhang Y. 2017. COFACTOR: improved protein function prediction by combining structure, sequence and protein-protein interaction information. *Nucleic Acids Research*, **45**, W291-W299.

Zhang H J, Lin Y P, Liu M, Liang X Y, Ji Y N, Tang B Z, Hou Y M. 2019. Functional conservation and division of two single-carbohydrate-recognition domain C-type lectins from the nipa palm hispid beetle *Octodonta nipae* (Maulik). *Developmental and Comparative Immunology*, **100**, 103416.

Zhang X, He Y, Cao X, Gunaratna R T, Chen Y R, Blissard G, Kanost M R, Jiang H. 2015. Phylogenetic analysis and expression profiling of the pattern recognition receptors: Insights into molecular recognition of invading pathogens in *Manduca sexta*. *Insect Biochemistry and Molecular Biology*, **62**, 38–50.

Zhang X W, Xu W T, Wang X W, Mu Y, Zhao X F, Yu X Q, Wang J X. 2009. A novel C-type lectin with two CRD domains from Chinese shrimp *Fenneropenaeus chinensis* functions as a pattern recognition protein. *Molecular Immunology*, **46**, 1626–1637.

Zheng J B, Mao Y, Su Y Q, Wang J. 2020. Identification of two novel C-type lectins involved in immune defense against white spot syndrome virus and *Vibrio parahaemolyticus* from *Marsupenaeus japonicus*. *Aquaculture*, **519**, 734797.

Zheng X, Xia Y. 2012. β-1,3-Glucan recognition protein (βGRP) is essential for resistance against fungal pathogen and opportunistic pathogenic gut bacteria in *Locusta migratoria manilensis*. *Developmental and Comparative Immunology*, **36**, 602–609.

Zhu Y T, Zhang X, Wang S C, Li W W, Wang Q. 2016. Antimicrobial functions of EsLecH, a C-type lectin, via JNK pathway in the Chinese mitten crab, *Eriocheir sinensis*. *Developmental and Comparative Immunology*, **61**, 225–235.

Executive Editor-in-Chief WAN Fang-hao
Managing Editor SUN Lu-juan